JOURNAL OF AIRCRAFT
Vol. 51, No. 6, November–December 2014

Engineering Notes

Stability of Aeroelastic Airfoils with Camber Flexibility

James R. Cook* and Marilyn J. Smith†
Georgia Institute of Technology, Atlanta, Georgia 30332

DOI: 10.2514/1.C032955

I. Introduction

MAXIMUM lift characteristics and vibratory loading of the rotor are limiting factors in rotorcraft performance [1]. To expand the range of helicopter capabilities, active control methods to improve performance and reduce vibratory loading are being developed. For example, Grohmann et al. [2] produced oscillatory trailing-edge deflections and active trailing-edge tabs by applying layers of piezoelectric fibers on the skin of an airfoil section and activating the piezoelectric fibers at frequencies ranging from $\omega/\Omega = 2$ to 6. In hover, aerodynamic pressures reduced the control authority by approximately 20%, indicating that aeroelastic effects must be included to produce an accurate aeroelastic analysis of the blade section. Gandhi et al. [3] designed and optimized a variable-camber blade section by integrating piezoelectric stacks into the blade structure and applying a compliant skin on the blade surface.

Highly compliant materials are applied in the construction of active airfoils to reduce the work required to deform the airfoil. Flexibility in camber can adversely affect the stability characteristics of a rotor blade. To determine the effects of camber flexibility on aeroelastic stability, Murua et al. [4] conducted a two-dimensional numerical aeroelastic experiment using the aerodynamic model of Peters et al. for flexible airfoils [5] and included pitch, plunge, and parabolic camber modes. Numerical results indicated that camber effects alone can cause flutter and that the camber mode significantly influences stability boundaries when coupled with pitch and plunge modes. In forward flight and during maneuvers, the increased presence of transonic flow, dynamic stall, and wake effects add to the complexity of the physics. Thus, the solution of the Navier–Stokes equations is required to obtain accurate performance characteristics.

The ability of a surface-conforming aeroelastic methodology formed from coupling an unsteady Reynolds-averaged Navier–Stokes (URANS) computational fluid dynamics (CFD) solver with a computational structural dynamics (CSD) code to predict pitch/plunge and parabolic camber flutter speeds of a thin symmetrical airfoil in incompressible and compressible flow is demonstrated in this work. This CFD/CSD method is believed to be one of the first approaches that includes full-surface morphing for rotating blades in the current published literature.

Received 18 April 2014; revision received 30 July 2014; accepted for publication 4 August 2014; published online 7 November 2014.

*Graduate Research Assistant, Daniel Guggenheim School of Aerospace Engineering.
†Professor, Daniel Guggenheim School of Aerospace Engineering.

II. Aeroelastic Methodology

The aeroelastic method couples a finite-element CSD code (University of Michigan's NLABS [6,7]) with a URANS CFD solver (NASA's FUN3D [8,9]) at each time step. The development and validation of this methodology is discussed in Cook [10] and Thepvongs et al. [11].

The fluid-structure interface applied in this effort was originally developed for three-dimensional morphing rotor blades [11] and has been modified for application to two-dimensional flexible airfoils [10]. In this methodology the aerodynamic forces on each cell face on the surface of the blade are imported into NLABS and interpolated onto an interface grid, based on an inverse isoparametric mapping (IIM) method [12]. These forces are applied in the structural model to compute beam deflections and cross-sectional deformations. Displacements are then interpolated at CFD grid nodes using the IIM method and exported to the CFD solver. Beam deflections were eliminated by increasing the bending and torsional stiffnesses to 10^{20} N · m^2, which effectively modeled a rigid blade in bending and torsion with deflections less than 10^{-6} chord. Substantiation of spatial and temporal independencies for the grids applied in this note has been demonstrated in Cook [10] and Thepvongs et al. [11].

To verify the methodology, the stability of an airfoil section was evaluated with both a single parabolic camber degree of freedom as well as with pitching and plunging degrees of freedom. The results for the parabolic camber flutter evaluation were compared with a closed-form approximate solution for a NACA 0012 airfoil, which is in accordance with thin airfoild theory, in the incompressible Mach range by Murua et al. [4]. This solution depends only on the inverse mass ratio $\kappa = \pi\rho_\infty b/m$. Results that include a lower-fidelity aerodynamics model (the finite state of Peters et al. [5]) and a URANS aerodynamics module with the Menter k-ω turbulence model [13] were compared. At higher mass ratios, the results of the two methods were comparable to the approximate solution, but at lower mass ratios, differences are observed in the results of potential-based linear aerodynamic methods and the nonlinear CFD simulations (Fig. 1a [14,15]). In potential-based methods, viscosity is neglected, airfoil deflections are assumed to be small relative to chord length, disturbance velocities are small compared to freestream velocity, and the wake is assumed to be one-dimensional. Differences in flutter speed, blade loading, and structural deflection predictions based on potential methods and CFD are further analyzed and discussed in Cook [10] and Thepvongs et al. [11].

A two-dimensional pitch–plunge flutter analysis with a rigid NACA 0012 airfoil was also evaluated. Comparisons with Theodorsen and Garrick [16], corrected by Zeiler [15], were compared with the two aerodynamic modules. In these cases, the location of the elastic axis, a, was −0.3 semichords aft the midchord; the inverse mass ratio $\kappa = \pi\rho_\infty b^2/m$, where ρ_∞ is the freestream air density, b is the semichord, and m is the blade mass per unit span, was 0.05; the radius of gyration, r_α, was 0.5; and center of mass, x_α, was varied at 0.0, 0.1, and 0.2 semichords aft of the elastic axis in F-S/NLABS simulations. In FUN3D/NLABS simulations, results were generated only for $x_\alpha = 0.1$. In each case, the flutter speed predictions were within 3% of those of Zeiler [15]. Results correlate well at $x_\alpha = 0.1$ (5% difference in the flutter speed) when $\omega_\xi/\omega_\alpha \leq 0.9$, whereas the CFD-based solution deviates up to 47% at larger natural frequency ratios ($\omega_\xi/\omega_\alpha = 1.4$, Fig. 1b). This difference at the larger frequency ratios is because the pitch mode begins to dominate the instability. The physical assumptions of the two aerodynamic models begin to deviate as the angle of attack increases.

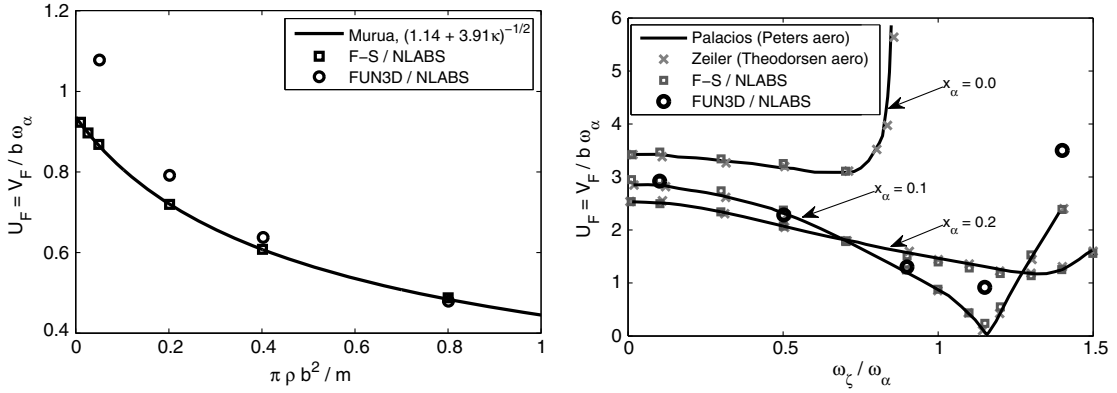

a) Camber mode b) Pitch-plunge modes

Fig. 1 Flutter speeds for camber and pitch–plunge modes for the NACA 0012 with comparisons to Murua [4], Palacios [14], and Zeiler [15].

III. Stability Analysis of Two-Dimensional Airfoil Sections

The finite-state/NLABS and URANS/NLABS analyses have also been applied to a NACA 23012 airfoil at compressible velocities to determine the minimum stiffness required for a flexible airfoil section. The airfoil is that of the rotor in the hover tip vortex structure test [17]. The torsion and flap stiffnesses (126 N · m/rad and 15.4 kN/m, respectively) were selected so that the natural frequencies correspond to the first natural frequencies of twist (415 rad/s) and flap (121 rad/s) of the rotor rotating at 109 rad/s.

Simulations were performed at three nondimensional freestream velocities $U_\infty = V_\infty/\omega_\delta b$ of 6.5, 8.7, and 10.8 ($M_\infty = 0.48$, 0.64, and 0.80, respectively). These correspond to the velocity at the rotor 75% radial station and tip in hover and the maximum tip velocity during forward flight at an advance ratio of $\mu = 0.25$. The inverse mass ratio is 0.0148, and the elastic axis and center of mass are located at the quarter-chord. Spatial and temporal independence were ensured by following the guidelines of studies performed previously on the NACA 0012 airfoil.

Results with finite-state aerodynamics indicate that static divergence due to camber–pitch coupling is encountered before the onset of flutter. The static deflections of the airfoil (Fig. 2) identify the minimum frequency ratios required for stability at $U_\infty = 6.5$, 8.7, and 10.8 to be approximately $\omega_\delta/\omega_\alpha = 12$, 24 and 72, respectively.

In cases where the flow remains subsonic ($M_\infty = 0.48$ and 0.64 at $0 < \alpha < -3$ deg), the pitch deflections of the finite-state/NLABS and FUN3D/NLABS simulations agree to within 10–12%. As stiffness decreases, the airfoil deflections increase, and the flow becomes transonic. The predictions of the two aerodynamic models begin to diverge, resulting in differences in the predicted pitch angles of greater than 41%, regardless of camber stiffness. In all cases (Figs. 2a and 2b), the magnitude of the mean pitch and camber deflections predicted by the finite-state aerodynamics are larger than those predicted by URANS.

Large airfoil deflections and transonic flow in the URANS simulations produce separation and shed vortices that introduce unsteady pressure loads that drive the oscillatory deflections. These vortices are not modeled by the finite-state aerodynamic model in NLABS, and as a consequence, the NLABS deflections were steady.

The load and deflections are further examined at $M_\infty = 0.64$ to understand the interaction between camber, pitch, and plunge modes. As the camber stiffness is decreased, pitch deflections become larger, and nonlinear aerodynamic effects cause unsteady airfoil loads resulting in limit-cycle oscillations at low frequencies due to the plunge mode and higher frequencies due to the pitch and camber modes. As camber stiffness is decreased, the camber deflections become larger and begin to dominate the physics. These high-frequency oscillations also drive pitch oscillations, while the plunge mode is damped [10].

A single camber oscillation period illustrates the influence of the transonic flow and separation vortices. Flow contours are examined at nondimensional time intervals $s = 0.9$, from 0.0 to 7.2 (Fig. 3), where $s = t(U_\infty/b)$. At $s = 1.8$, a vortex forms on the lower surface of the airfoil due to the large camber deflection (Fig. 3c). As the vortex travels along the lower side of the airfoil, it creates a low-pressure region near the midchord, driving a negative camber deflection (Fig. 3, $s = 2.7$–4.5). At the same time, a shock forms at $60\%c$ on the upper surface and moves forward until it reaches the leading edge (Fig. 3b, $s = 2.7$–6.3). The shock induces boundary-layer separation, resulting in a new vortex on the upper surface of the airfoil (Fig. 3c).

As this vortex passes the midchord of the airfoil, it creates a low-pressure region on the upper surface, which drives a positive camber deflection (Fig. 3d, $s = 6.3$–7.2, $s = 0.0$–1.8). At $s = 1.8$, the

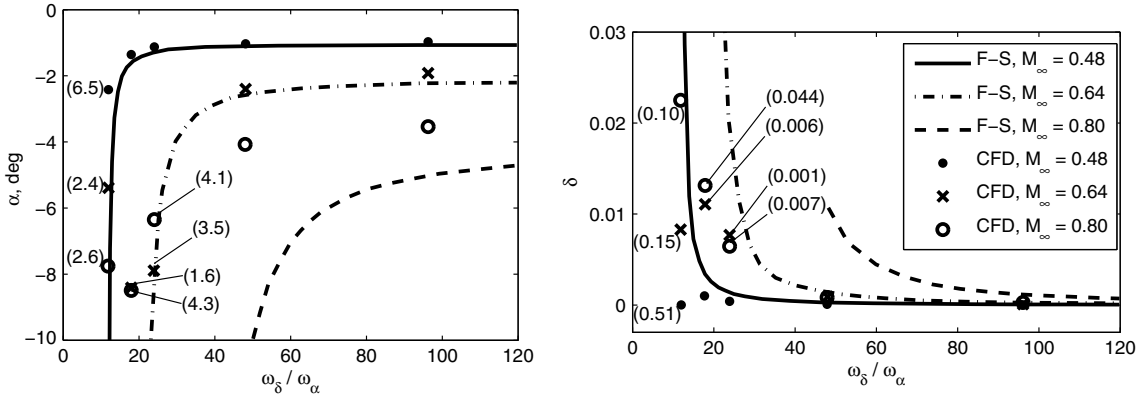

a) Pitch b) Camber

Fig. 2 Mean deflections for NACA 23012 airfoil. The amplitude of unsteady deflections is indicated in parentheses when present. The response was steady for all cases when finite-state aerodynamics were used.

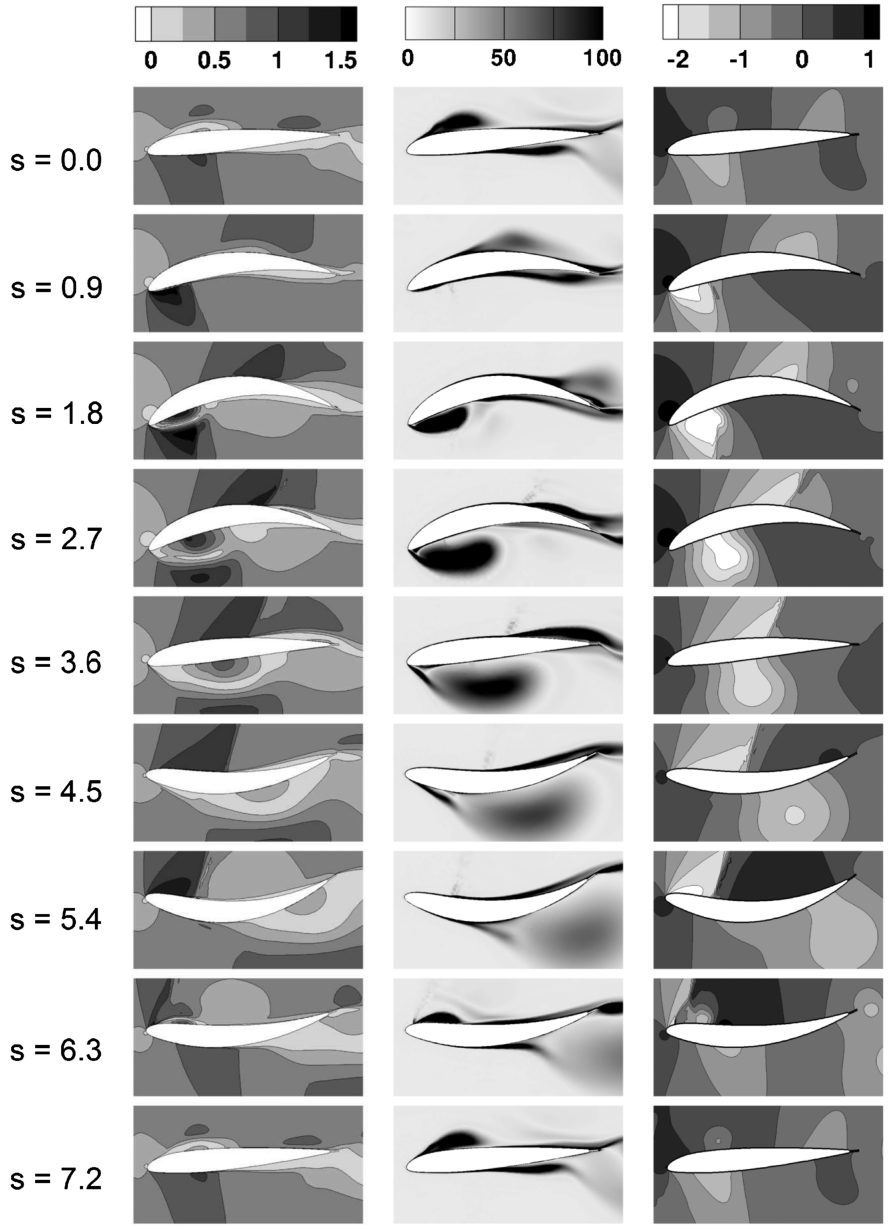

Fig. 3 Mach, vorticity, and pressure contours for $M_\infty = 0.64$, $\omega_\delta/\omega_\alpha = 12.0$; $s = 0$ for top images and 7.2 for bottom images with step of $\Delta s = 0.9$ between images.

vortex on the upper surface reaches the trailing edge as another vortex forms on the lower surface at the leading edge, and the cycle repeats.

IV. Conclusions

Two-dimensional aeroelastic analyses of a flexible symmetric airfoil in incompressible and compressible flow have been performed using a CSD solver, with aerodynamics based on finite-state flexible thin airfoil theory and a coupled URANS CFD/CSD methodology. In the incompressible cases, the CFD/CSD methodology is verified through comparison to analytical solutions for camber stability based on finite-state theory. The following conclusions can be made.

1) At high inverse mass ratios, the prediction of the flutter speeds by both methods for the camber mode compare well. The finite-state aeroelastic flutter speed solutions are lower at very low inverse mass ratios due to the different physical assumptions in the two aerodynamics models. For the finite-state aerodynamic analysis, this includes small perturbations, inviscid flow, and a linear wake.

2) Predicted flutter speeds using URANS and finite-state aerodynamic models for a pitching and plunging airfoil are comparable when the instability is dominated by the plunge mode. As the plunge-to-pitch frequency ratio $\omega_\zeta/\omega_\alpha$ increases, the instability is dominated by pitching motion, which the finite-state-based aeroelastic method cannot accurately capture and results in a lower flutter speed prediction.

3) In compressible subcritical subsonic flow, finite-state-based aeroelastic solutions predict 10–12% larger pitch deflections, whereas the URANS aeroelastic stability limits agree with classic thin airfoil theory. In transonic conditions finite-state-based aeroelastic simulations predicted much larger pitch deflections in all cases due to the lack of aerodynamic damping inherent in URANS.

4) A novel CFD/CSD coupling method has successfully predicted limit-cycle oscillations of an airfoil when transonic flow and leading-edge separation are present. Finite-state aerodynamics were not capable of modeling these nonlinear aerodynamic phenomena.

Acknowledgments

This effort was sponsored in part by the Vertical Lift Center of Excellence at the Georgia Institute of Technology. Michael

Rutkowski was the technical monitor of this center. Computational support was provided through the U.S. Department of Defense High Performance Computing Centers at Naval Oceanographic Office through an High-Performance Computing grant from the U.S. Army. Roger Strawn is the Service/Agency Approval Authority of this grant. The computer resources of the U.S. Department of Defense Major Shared Resource Centers are gratefully acknowledged. Opinions, interpretations, conclusions, and recommendations are those of the authors and are not necessarily endorsed by the U.S. Government. The authors would like to thank Devesh Kumar for assistance in generating the NLABS input decks used for the NLABS simulations.

References

[1] Ormiston, R. A., "Applications of the Induced Power Model and Performance of Conventional and Advanced Rotorcraft," *Proceedings of the AHS Aeromechanics Specialists Conference*, American Helicopter Soc., Alexandria, VA, Jan. 2010, pp. 588–615.

[2] Grohmann, B. A., Müller, F., Ahci, E., Pfaller, R., Bauer, M., Maucher, C., Dieterich, O., Storm, S., and Jänker, P., "Design, Evaluation and Test of Active Trailing Edge," *Proceedings of the American Helicopter Society 67th Annual Forum*, American Helicopter Soc., Alexandria, VA, May 2011, pp. 1079–1104.

[3] Gandhi, F., Frecker, M., and Nissly, A., "Design Optimization of a Controllable Camber Rotor Airfoil," *AIAA Journal*, Vol. 46, No. 1, 2008, pp. 142–153. doi:10.2514/1.24476

[4] Murua, J., Palacios, R., and Peiró, J., "Camber Effects in the Dynamic Aeroelasticity of Compliant Airfoils," *Journal of Fluids and Structures*, Vol. 26, No. 4, 2010, pp. 527–543. doi:10.1016/j.jfluidstructs.2010.01.009

[5] Peters, D. A., Hsieh, M.-C. A., and Torrero, A., "A State-Space Airloads Theory for Flexible Airfoils," *Journal of the American Helicopter Society*, Vol. 52, No. 4, 2007, pp. 329–342. doi:10.4050/JAHS.52.329

[6] Palacios, R., and Cesnik, C. E. S., "Geometrically Nonlinear Theory of Composite Beams with Deformable Cross Sections," *AIAA Journal*, Vol. 46, No. 2, 2008, pp. 439–450. doi:10.2514/1.31620

[7] Palacios, R., and Cesnik, C. E. S., "Cross-Sectional Analysis of Nonhomogeneous Anisotropic Active Slender Structures," *AIAA Journal*, Vol. 43, No. 12, 2005, pp. 2624–2638. doi:10.2514/1.12451

[8] Anderson, W., Rausch, R., and Bonhaus, D., "Implicit/Multigrid Algorithms for Incompressible Turbulent Flows on Unstructured Grids," *Journal of Computational Physics*, Vol. 128, No. 2, 1996, pp. 391–408. doi:10.1006/jcph.1996.0219

[9] Bonhaus, D., "An Upwind Multigrid Method for Solving Viscous Flows on Unstructured Triangular Meshes," M.S. Thesis, George Washington Univ., Washington, D.C., 1993.

[10] Cook, J. R., "Development of an Aeroelastic Methodology for Surface Morphing Rotors," Ph.D. Thesis, Georgia Inst. of Technology, Atlanta, 2014.

[11] Thepvongs, S., Cesnik, C. E. S., Cook, J. R., and Smith, M. J., "Computational Aeroelasticity of Rotating Wings with Deformable Airfoils," *Proceedings of the American Helicopter Society 65th Annual Forum*, American Helicopter Soc., Alexandria, VA, April–May 2009.

[12] Pidaparti, R. M. V., "Structural and Aerodynamic Data Transformation Using Inverse Isoparametric Mapping," *Journal of Aircraft*, Vol. 29, No. 3, 1992, pp. 507–509. doi:10.2514/3.46190

[13] Menter, F. R., "Two-Equation Eddy-Viscosity Turbulence Models for Engineering Applications," *AIAA Journal*, Vol. 32, No. 8, Aug. 1994, pp. 1598–1605. doi:10.2514/3.12149

[14] Palacios, R., and Cesnik, C. E. S., "Low-Speed Aeroelastic Modeling of Very Flexible Slender Wings with Deformable Airfoils," *49th AIAA/ASME/ASCE/AHS/ASC Structures, Structural Dynamics and Materials Conference*, AIAA Paper 2008-1995, April 2008.

[15] Zeiler, T. A., "Results of Theodorsen and Garrick Revisited," *Journal of Aircraft*, Vol. 37, No. 5, Sept.–Oct. 2000, pp. 918–920. doi:10.2514/2.2691

[16] Theodorsen, T., and Garrick, I. E., "Flutter Calculations in Three Degrees of Freedom," NACA TR-741, 1941.

[17] Van der Wall, B. G., and Richard, H., "Hover Tip Vortex Structure Test (HOTIS)—Test Documentation and Representative Results," DLR, German Aerospace Center, TR-IB-111-2008/16, Braunschweig, Germany, May 2008.